Continuously tunable microdroplet-laser in a microfluidic channel

Continuously Tunable Droplet-based Optical Microcavities

Sindy K. Y. Tang[1,*], Ratmir Derda[1,2], Qimin Quan[2,3], Marko Loncar[3], and George M. Whitesides[1,*]

[1]*Department of Chemistry and Chemical Biology, Wyss Institute for Biologically Inspired Engineering, Harvard University, Cambridge, MA 02138.*

[3] *School of Engineering and Applied Sciences, Harvard University, Cambridge, MA 02138.*

[2] *These authors contributed equally to this work.*

**tang@fas.harvard.edu*

**gwhitesides@gmwgroup.harvard.edu*

Abstract:

This paper describes the generation and optical characterization of a series of dye-doped droplet-based optical microcavities with continuously decreasing radius in a microfluidic channel. A flow-focusing nozzle (FFN) generated the droplets (~ 21 μm in radius) using benzyl alcohol as the disperse phase and water as the continuous phase. As these drops moved down the channel, they dissolved, and their size decreased. The emission characteristics from the drops could be matched to the whispering gallery modes from spherical micro-cavities. The wavelength of emission from the drops changed from 700 to 620 nm as the radius of the drops decreased from 21 μm to 7 μm. This range of tunability in wavelengths was larger than that reported in previous work on droplet-based cavities.

1. Introduction

In a micro-spherical cavity, light is confined by total internal reflections at the interface between the microsphere and the medium that surrounds it. Electromagnetic waves—coupled into the cavity or emitted from a gain medium inside the cavity—that meet the requirements for constructive interference form standing waves. The energy stored in the cavity at these frequencies increases. These waves are the resonance modes of the cavity; they are also called the whispering gallery modes (WGMs). We and others have demonstrated enhancement of light and lasing in WGMs from microcavities made of droplets [1-8]. Microdroplets—with their small sizes, and with their surfaces made spherical and smoothed by surface tension—are effective optical microcavities. Microfluidics droplet technology (based on flow-focusing nozzles, T-junctions, and other structures) allows convenient generation of large numbers of monodisperse drops at rates > 10 kHz [9]. The diameters of drops produced are usually in the range of tens of microns [10]. This length scale is well-suited for studies of whispering gallery modes in the visible and near-infrared wavelengths. By combining two microfluidic T-junctions for alternate generation of drops containing different types of dye solutions, we demonstrated switching of lasing wavelengths between 580 nm and 680 nm at frequencies up to 3.6 kHz, the fastest for a reported dye laser [2]. These drop-based dye lasers have the potential to be useful in combination with other microfluidic components for on-chip spectroscopy applications.

This paper extends the idea of wavelength tuning in droplet-based dye lasers by using droplet cavities whose size decreases continuously after generation. We formed drops using two liquids—benzyl alcohol for the drops, water for the carrier fluid—that were partially miscible with each other. As the drops traveled downstream, they dissolved into the carrier fluid and decreased in size. The time for the drops to dissolve completely was similar to the residence

time of the drops in the channel. A large range of sizes of drops was therefore present in the channel at any time. At fixed positions in the channel, the size of the drops was fixed. By positioning the excitation laser at different parts of the channel, we were able to interrogate the optical properties of droplet cavities possessing different sizes.

We observed that the emission wavelengths from the droplet cavities changed over a large range (~ 80 nm) as the radius of the cavities decreased from 21 μm to 7 μm. This range was larger than that reported in previous studies of droplets evaporating in air (< 10 nm) [1, 8]. Selection of the size of the droplets according to their position in the channel made it possible to select the wavelengths of emission over this ~ 80 nm range. The rate at which wavelengths could be tuned or selected was relatively slow in the device we describe (~ seconds), but could be reduced to milliseconds using a rapidly steerable excitation beam. As the drops decreased in size, the refractive index of the drops and the concentration of dye solutions in the drops also changed. We show that these effects were, however, much smaller than that due to the decrease in the size of the drops in causing the change in emission characteristics from the drops.

2. Experimental Design

2.1 Microchannel design

We fabricated a flow-focusing nozzle (FFN) [9] to generate droplets in poly(dimethylsiloxane) (PDMS) using soft lithography [11]. Other structures for generating drops, such as T-junctions [12], could also be used. The height of the channel was 40 μm. The length of the channel was 16 cm, and the width of the channel decreased from 60 μm to 20 μm continuously (Figure 1a). Using channels with tapered width kept the drops centered as they decreased in size. The long

channel was necessary to allow sufficient time for the drops to dissolve into the carrier fluid, and, thus, to change size sufficiently to change the wavelength of emission over a useful range. In the simple constructed device we used, we were unable to cause fluids to flow through a channel longer than 16 cm due to the high fluidic resistance to fluid flow. At the pressure that would have been required to produce usefully rapid flows through long channels, the tubings used to bring fluids to the FFN and channel detached from the inlets of the PDMS device. It should be possible to solve this problem by using a different method of connection to the channel, a microfluidic system of different design, or by applying vacuum to the outlet of the channel to assist the flow in channels longer than 16 cm. We have not demonstrated these capabilities in this work.

2.2 Choice of fluids

To form droplet microcavities, we used 1 mM solution of rhodamine 640 perchlorate in benzyl alcohol (n_{drop} = 1.54) as the disperse phase, and water ($n_{carrier}$ = 1.33) with 0.5 % sodium dodecyl sulfate (SDS) as the continuous phase. Rhodamine was the gain medium. SDS was necessary to facilitate stable generation of the drops, and to prevent the drops from wetting the walls of the channel. In principle, other pairs of liquids could also be used so long as they satisfy four requirements: (i) The contrast in refractive index between the drop and the carrier fluid must be sufficiently high to allow confinement of light for lasing in whispering gallery modes in droplets with radius studied. The contrast in index here was Δn = 0.21, and the radius of the drops was between 21 μm and 7 μm. A list of refractive indices for common liquids can be found in the supplementary information in [13]. (ii) The disperse phase must dissolve the laser dye readily. Rhodamine 640 perchlorate was soluble in benzyl alcohol up to 0.591 g/mL. (iii) The capillary number characterizing the importance of viscous forces over interfacial forces (Ca = $u\eta/\gamma$, u is

the characteristic speed of the liquids, η is dynamic viscosity of the liquids, and γ is the interfacial tension between the disperse and continuous phases) must be sufficiently low to allow stable generation of monodisperse drops at the FFN [14]. Monodispersity in the size of the drops also ensures a uniform dissolution rate of the drops, and that the drops had the same size at fixed positions downstream in the channel. The Ca number in our system was about 0.04. (iv) The liquids must be partially miscible with each other. The solubility limit of benzyl alcohol in water was 4 wt %, and that of water in benzyl alcohol was 8 wt %.

We used a syringe pump to introduce liquids into the microchannel. We fixed the rates of flow of the continuous phase at 200 μL h^{-1}, and that of the disperse phase at 20 μL h^{-1} for all experiments unless stated otherwise. The drops produced by the FFN always had the same radius (~ 21 μm, < 1% polydispersity). The rate of generation was constant at ~ 125 drops/second; this rate could be increased to over 1000 drops/second, if desired, by using higher rates of flow. For some control experiments, we formed drops from benzyl alcohol that was saturated with water, in a carrier liquid of water that was saturated with benzyl alcohol. These drops did not dissolve into the carrier liquid and their size did not change as they traveled in the channel. Using this combination of liquids, we were able to study the effects of parameters such as the concentration of dye solution in the drops independent of the size of the drops [15].

2.3 Optical excitation and measurements

We mounted the microfluidic device on an inverted microscope (Figure 1b). We used a pulsed, frequency-doubled Nd:YAG laser at 532 nm as the excitation source. The pulse width was about 20 ns. The pump beam was coupled into the microscope and focused at the microchannel with a beam diameter of ~ 30 μm. The repetition rate of the laser was 1 kHz. At this repetition rate,

each drop was excited at least once as the residence time of drops in the pump spot was ≥ 1 ms. We did not observe photobleaching of the dye since the drops were flowing continuously and we excited each drop once only. To characterize the emission from the drops, we varied the pump pulse energy from 0.01 to 100 J-cm^{-2}. We collected light emitted from the drops using a 20x objective (numerical aperture NA = 0.4) normal to the plane of the microchannel (in the *z*-direction). The light was coupled to a spectrometer for characterization using an optical fiber. Since the focal point of the excitation source was fixed in our setup, in order to select and examine drops with different sizes, we adjusted the position of the device using a manual translation stage on the microscope to bring different parts of the channel into the focus of the excitation beam.

3. Results and Discussions

3.1 Generation of droplet resonators with continuously decreasing sizes

We recorded movies of the drops in the channel using a fast camera (at 5000 frames/s) and measured the radius of the drops at different locations downstream from the FFN. The drops travelled through a 16-cm long channel in ~ 3.5 seconds (Figure 2). During this time, the radius of the drops decreased from 22 μm to less than 5 μm. While the kinetics and mathematical model of the dissolution of droplets flowing in a narrow microchannel has not been reported, we found that the decrease in the size of the drops could be described by first-order kinetics with respect to the surface area of the droplet at a rate constant of 0.92 s^{-1} (Figure 2c). This observation is similar to that reported for the dissolution of CO_2 bubbles in a microchannel [16]. From the first-order kinetics fit, we extrapolated that droplets with radius of 20 μm would reach

sub-micron size in approximately 8 seconds in our system. It was difficult to observe this decrease in radius in our experimental setup, however. At average droplet speed of 4 to 5 cm s^{-1}, a 30- to 40-cm channel would be necessary to obtain sub-micron droplets; the corresponding fluidic resistance would be too high to drive fluids through this channel.

3.2 Identification of WGM modes from the lasing spectrum

We first characterized the optical properties from drops possessing a fixed size. For this experiment only, we increased the rate of flow of the continuous phase to 400 μL h^{-1} and generated drops with radius ~ 17.4 μm. We measured light emitted from the drops within 50 μm from the FFN before much dissolution of the drop occurred.

Figure 3 shows the emission characteristics from the drops when excited below and above lasing thresholds. When excited by a pump beam with power below the threshold for lasing, we observed fluorescence from the drop where the pump beam was focused (Figure 3ai). The emission spectrum was similar to the bulk fluorescence of the dye (dashed in Figure 3c,d). At pump powers above the lasing threshold (> 2 μJ/pulse, inset in Figure 3d), we observed a ring of high intensity around the circumference of the drop (Figure 3aii), similar to that reported in previous droplet lasing experiments [5]. The emission spectrum exhibited multiple modes or peaks in intensity from 660 nm – 675 nm (Figure 3d). The spacing between the lasing modes was 2.7 nm, corresponding to a free spectral range (FSR) of ~ 1.8 x 10^{12} Hz.

The theoretical description of the lasing conditions for WGM modes has been described previously [7]. Qualitatively, modes lase when the gain is larger or equal to the loss due to absorption of the dyes, and radiative loss of light out of the droplet. Since the absorption and

gain spectrum of rhodamine overlaps from ~ 550 nm to 620 nm (Figure 3c), lasing tends to occur at the long-wavelength end of the gain spectrum > 620 nm.

WGMs from microspheres can be characterized by three numbers: *p, m* and *l*, for both TE (transverse electric) and TM (transverse magnetic) polarizations [7]. The *p, m,* and *l* numbers are integers, and they represent the distribution of intensity of the resonant modes inside a sphere. *p* indicates the number of peaks in intensity inside the sphere in the radial direction. *m* indicates the number of peaks along the circumference of the sphere in the direction of circulation of the WGMs, and $l - m + 1$ indicates the number of peaks in the azimuthal direction. We compared the positions of the observed lasing modes to theoretical values calculated for passive micro-spherical resonators using an explicit asymptotic formula [17-18] (Appendix A5). We found that these modes could be matched to those belonging to a spherical cavity with radius R = 17.352 μm, n_{drop} = 1.54, $n_{carrier}$ = 1.33. These modes were transverse magnetic (TM) in nature, and they corresponded to mode order p = 1, and mode numbers $m = l$ = 238 to 244. Lasing of p = 1 modes have also been observed before [7-8]. The measured linewidth of the modes was 0.16 nm (Figure 3d), close to the detection limit of the spectrometer (0.1 nm). This linewidth indicates that the quality factor of the modes was at least 4×10^3.

3.3 Blue-shift in emission wavelengths as the drops decreased in size

Figure 4a shows a series of emission spectra from drops possessing different sizes obtained at different positions in the channel (Figure 2). The pulse energy of the pump beam was fixed at 0.24 mJ/pulse. We made three observations, as the drops decreased in size: (i) The wavelengths of the emitted light from the drops shifted from ~ 700 nm to ~ 620 nm as the radius of the drops decreased from 21 μm to 7 μm. (ii) The free spectral range (FSR)—measured from the spacing

between consecutive modes in the emission spectrum—increased (Figure 4b). (iii) The number of lasing modes decreased.

As the drops dissolved into the carrier fluid, three parameters changed: (i) The contrast in the refractive index between the drop and the carrier fluid decreased. (ii) The concentration of the dye solution in the drops increased. (iii) The radius of the droplet cavity decreased. We examine the effects of each below.

3.3.1 Effect of decreased contrast in index of refraction between the drop and the carrier fluid

As benzyl alcohol dissolved into water, the refractive index of the continuous phase increased and that of the disperse phase decreased. Since the solubility limit of benzyl alcohol in water is 4%, the maximum refractive index of the continuous phase would be 1.34 (0.75 % increase from 1.33). Water also dissolves in benzyl alcohol up to 8 wt %. The minimum refractive index of the drops would be 1.52 (1.3% decrease from 1.54). We also confirmed these values experimentally: the measured index of water saturated with benzyl alcohol was 1.34, and that of benzyl alcohol saturated with water was 1.52. Using the asymptotic formula in [17] (Appendix, A5), we estimated that the decrease in the contrast of refractive index between the drop and the carrier liquid would cause the positions of the WGMs to decrease ~ 5 nm. This change was insignificant compared with the shift over 80 nm observed in Figure 4.

3.3.2 Effect of increased concentration of dye

The concentration of the rhodamine solution in the drops increased as the volume of the drops decreased. We measured the partition coefficient of rhodamine 640 perchlorate between benzyl alcohol and water at equilibrium to be $K_{bw} = [dye]_{benzyl\ alochol}/[dye]_{water} \sim 20000$. Because of this large value of K_{bw}, most of the dye molecules remained in benzyl alcohol. While we could not

quantify the concentration of rhodamine solution inside the drops dynamically, the concentration should scale inversely with the volume of the drop. With the reduction in the volume of the drops in our experiments ($V_{initial}$ ~ 125 V_{final}, corresponding to a decrease in radius of ~ 5 fold), the highest concentration of rhodamine solution in the drop would be ~ 125 mM, much lower than the solubility limit of rhodamine in benzyl alcohol (which we estimated to be at least 1 M). We did not expect, and did not observe, any aggregation or precipitation of dye molecules inside the drops as they decreased in volume.

To study the effect of different concentrations of dye solutions in the drops, we measured the emission spectra from drops at a fixed size (radius ~ 16.9 μm) containing different concentrations of dye. We generated drops containing solutions of dye in benzyl alcohol that was saturated with water in a carrier fluid comprising water saturated with benzyl alcohol. These drops did not dissolve into the carrier fluid, and their size remained constant as they travelled downstream. Using this system, we were able to determine the effect of the concentration of the dye solution independent of the size of the drops. We found that the emission wavelengths increased from ~ 660 nm to 700 nm as the concentration of rhodamine increased from 1 mM to 96 mM (data not shown). We therefore conclude that the increase in the concentration of the dye solution as the drops decreased in volume could not have caused the observed blue-shift in lasing wavelengths.

3.3.3 Effect of decreased radius of the drops

For WGMs of a fixed set of *p*, *m*, and *l* numbers, the change in the wavelengths of WGMs is directly proportional to the change in the size of the cavity: $\Delta\lambda_{p,m,l} / \lambda_{p,m,l} = \Delta R/R$ [1]. This relation does not apply to our system: the blue-shift in wavelengths would have been ~ 450 nm,

much larger than the observed 80 nm, when the radius of the drops decreased from 21 μm to 7 μm. The WGMs from drops with different sizes observed in our experiment, therefore, could not belong to the same set of *p*, *m* and *l* numbers.

We attempt to provide a qualitative explanation for the changes in the wavelengths of emission based on the output power from the droplet cavities. In a microspherical cavity, light emitted from the gain medium either couples outside the cavity, or is absorbed by the medium. The efficiency (β) of out-coupling of light from the cavity to free space can therefore be expressed as the ratio of the radiative quality factor Q_{rad} to the effective quality factor Q_{total} of the cavity, which accounts for both radiative loss (Q_{rad}) and absorption loss (Q_{abs})in the cavity [7]:

$$\beta = \frac{Q_{rad}^{-1}}{Q_{total}^{-1}} = \frac{Q_{rad}^{-1}}{Q_{rad}^{-1} + Q_{abs}^{-1}} \qquad (1)$$

The power P_o of lasing light coupled out of the cavity (i.e. the power that can be measured) can also be estimated following equation 6 in [7]:

$$P_o \sim \frac{V(R,\lambda)}{\lambda^3} g(\lambda)\beta(\frac{R}{\lambda}) \qquad (2)$$

where V is the optical mode volume of the cavity, g is gain spectrum of the dye, R is the radius of the cavity, and λ is the wavelength of emission.

At wavelengths longer than the peaks of absorption and gain spectrum (~ 600 nm in our experiments, Figure 3c), light at longer wavelengths experiences smaller absorption loss than light at shorter wavelengths; they are also less confined by a spherical cavity by total internal reflection. As a result, the efficiency of out-coupling of light from the cavity β increases with wavelength (Figure 5a). On the other hand, g and V/λ^3 decrease as wavelength increases (Figure 5b). It is then trivial to show that $P_o(\lambda)$—the product of an increasing function and decreasing

functions— must consist of a maximum (Figure 5c). This maximum value is the peak out-coupled laser power, and should correspond to the wavelengths of the observed lasing modes.

As the radius of the cavity decreases, the gain spectrum remains the same since it depends on the properties of the gain medium (dye) only. Mode volume V decreases as R decreases. The out-coupling efficiency β increases as R decreases, however, since smaller cavities are less able to confine light by total internal reflection than larger cavities. The wavelength at which maximum output power occurs, therefore, shifts to short wavelengths as the cavity decreases in size (Figure 5c). The wavelengths at which lasing can be observed should blue-shift correspondingly.

Figure 5c shows the calculated output powers for two sizes of droplets using equation 6 in [7]. From the calculations, the peak output power for drops with R = 19.4 μm occurred at about 700 nm; while that for drops with R = 8.9 μm occurred at about 600 nm. This blue-shift of 100 nm was close to that observed in Figure 4a. The exact wavelengths of the peak output powers were different from the observed lasing wavelengths by ~ 20 nm. We believe part of this difference originated from small errors in the values of the gain spectrum we used. The width of these calculated output power spectra was larger than that observed experimentally. For example, the calculation for drops at R = 8.9 μm implies the lasing power would be non-zero at wavelengths up to 680 nm, while the lasing modes in our experiment occurred between 620 nm and 640 nm only. This discrepancy arises from the fact that the calculations here did not account for effects such as mode clamping or mode competitions, which decrease the number of WGM modes allowed to lase.

The change in the size of the drops also explains the observed changes in the free spectral range (FSR) and the number of lasing modes. For modes belonging to the same p number and

consecutive m numbers, FSR can be expressed as: $FSR = c/2\pi n_{eff}R$, where c is the speed of light, and n_{eff} is the effective refractive index of the WGM mode; n_{eff} was 1.48 extracted from the fit to the data in Figure 4b. Modes in smaller drops therefore have free spectral ranges larger than those in bigger drops. In addition, Q_{rad} is approximately proportional to the size parameter x of the cavity (defined as $x = 2\pi R/\lambda$) (Appendix A4, [7]). Modes in smaller drops thus have lower Q_{rad} than in bigger drops; the lower quality factors make these modes more difficult to lase. The number of lasing modes observed from smaller drops was, as a result, fewer than the number observed from bigger drops.

4. Conclusions

We have demonstrated a droplet-based dye laser with a large range of tunability in its emitted wavelengths. Since a continuum of droplet cavities with continuously decreasing sizes was present in the channel, adjusting the position of the channel relative to the excitation beam allowed the selection and tuning of the emission wavelengths. The changes in emission wavelengths were due to changes in the size of the droplet cavities; effects due to changes in the indices of refraction and the concentration of the dye solution were insignificant. Lasing modes from the drops matched closely with the whispering gallery modes from spherical cavities. Possible deformations in the shape of the drops due to flow-induced shear in the microchannel did not affect the sphericity of the plane at which the whispering gallery modes were observed. We did not observe single-mode lasing in the smallest drops we generated ($R \sim 7$ μm). It should, however, be possible to obtain single-mode lasing as the radius of drops decreased further [3].

Our method of generating droplet micro-cavities whose diameters decrease continuously was simple. It was more convenient than applying different rates of flow of the liquids. Applying different rates of flow usually requires time (up to tens of seconds or even minutes) for equilibration of flow after each change in the rate of flow. Many pairs of fluids that have limited mutual solubility can be used for our strategy, which does not rely on the characteristics of the drop generator, and should be compatible with any method for droplet generation. Further, it is possible to obtain drops of sub-micron sizes, if desired, and to increase the dissolution rate of the drops, by decreasing the volume fraction of the drops generated, or by incorporating additional continuous phase downstream.

The droplet cavities we described here can be useful as a tunable light source in combination with other microfluidic functionalities. In addition, with the increasing use of droplets as micro-compartments in microfluidic systems for studies in chemistry and biology [19], the investigation of optical properties of these droplets as optical microcavities can lead to the development of useful intra-cavity sensing schemes to monitor biochemical processes occurring inside the drops.

Acknowledgement

We thank Howard Stone for helpful discussions. This work was funded by DARPA award number W911NF-07-10647. A portion of this work was supported by NSF NIRT award number ECCS-0708905. Device fabrication was performed at the Center for Nanoscale Systems at Harvard.

References

1. H. M. Tzeng, K. F. Wall, M. B. Long, and R. K. Chang, "Evaporation and condensation rates of liquid droplets deduced from structure resonances in the fluorescence spectra," Opt. Lett. **9**, 273-275 (1984).

2. S. K. Y. Tang, Z. Li, A. R. Abate, J. J. Agresti, D. A. Weitz, D. Psaltis, and G. M. Whitesides, "A multi-color fast-switching microfluidic droplet dye laser," Lab Chip **9**, 2767-2771 (2009).

3. J. Schäfer, J. P. Mondia, R. Sharma, Z. H. Lu, A. S. Susha, A. L. Rogach, and L. J. Wang, "Quantum Dot Microdrop Laser," Nano Lett. **8**, 1709-1712 (2008).

4. M. Saito, H. Shimatani, and H. Naruhashi, "Tunable whispering gallery mode emission from a microdroplet in elastomer," Opt. Express **16**, 11915-11919 (2008).

5. S. X. Qian, J. B. Snow, H. M. Tzeng, and R. K. Chang, "Lasing droplets: highlighting the liquid-air interface by laser emission," Science **231**, 486-488 (1986).

6. H. B. Lin, A. L. Huston, B. L. Justus, and A. J. Campillo, "Some characteristics of a droplet whispering-gallery-mode laser," Opt. Lett. **11**, 614-616 (1986).

7. H. B. Lin, J. D. Eversole, and A. J. Campillo, "Spectral properties of lasing microdroplets," J. Opt. Soc. Am. B Opt. Phys. **9**, 43-50 (1992).

8. A. Kiraz, A. Kurt, M. A. Dündar, and A. L. Demirel, "Simple largely tunable optical microcavity " Appl. Phys. Lett. **89** (2006).

9. P. Garstecki, I. Gitlin, W. DiLuzio, G. M. Whitesides, E. Kumacheva, and H. A. Stone, "Formation of monodisperse bubbles in a microfluidic flow-focusing device," Appl. Phys. Lett. **85**, 2649-2651 (2004).

10. P. Garstecki, H. A. Stone, and G. M. Whitesides, "Mechanism for Flow-Rate Controlled Breakup in Confined Geometries: A Route to Monodisperse Emulsions," Phys. Rev. Lett. **94**, 164501/164501-164501/164504 (2005).

11. J. C. McDonald, D. C. Duffy, J. R. Anderson, D. T. Chiu, H. Wu, O. J. Schueller, and G. M. Whitesides, "Fabrication of microfluidic systems in poly(dimethylsiloxane)," Electrophoresis **21**, 27-40 (2000).

12. P. Garstecki, M. J. Fuerstman, H. A. Stone, and G. M. Whitesides, "Formation of droplets and bubbles in a microfluidic T-junction-scaling and mechanism of break-up," Lab Chip **6**, 437-446 (2006).

13. S. K. Y. Tang, C. A. Stan, and G. M. Whitesides, "Dynamically reconfigurable liquid-core liquid-cladding lens in a microfluidic channel," Lab Chip **8**, 395-401 (2008).

14. W. Lee, L. M. Walker, and S. L. Anna, "Role of geometry and fluid properties in droplet and thread formation processes in planar flow focusing," Phys. Fluids **21**, 032103/032101-032103/032114 (2009).

15. To prepare the saturated solutions, we mixed 1:1 ratio of benzyl alcohol and water. We stirred the mixture for 30 min at 60 degree C. We then centrifuged the mixture, and extracted the top phase (water saturated with benzyl alcohol) and bottom phase (benzyl alcohol saturated with water).

16. J. I. Park, Z. Nie, A. Kumachev, and E. Kumacheva, "A microfluidic route to small CO2 microbubbles with narrow size distribution," Soft Matter **6**, 630-634 (2010).

17. C. C. Lam, P. T. Leung, and K. Young, "Explicit asymptotic formulas for the positions, widths, and strengths of resonances in Mie scattering," J. Opt. Soc. Am. B **9**, 1585-1592 (1992).

18. J. D. Eversole, H. B. Lin, A. L. Huston, A. J. Campillo, P. T. Leung, S. Y. Liu, and K. Young, "High-precision identification of morphology-dependent resonances in optical processes in microdroplets," J. Opt. Soc. Am. B Opt. Phys. **10**, 1955-1968 (1993).

19. J. Clausell-Tormos, D. Lieber, J.-C. Baret, A. El-Harrak, O. J. Miller, L. Frenz, J. Blouwolff, K. J. Humphry, S. Koester, H. Duan, C. Holtze, D. A. Weitz, A. D. Griffiths, and C. A. Merten, "Droplet-Based Microfluidic Platforms for the Encapsulation and Screening of Mammalian Cells and Multicellular Organisms," Chem. Biol. **15**, 427-437 (2008).

20. S. J. Adams, *Electromagnetic Theory* (Adams Press, 2008).

Appendix

Following definitions from [20], the transverse magnetic (TM) mode refers to the mode that has major radial component of electric field, and the eigenmode equation is:

$$\frac{[n_1 kRj_l(n_1 kR)]'}{n_1{}^2 j_l(n_1 kR)} = \frac{[n_2 kRh_l(n_2 kR)]'}{n_2{}^2 h_l(n_2 kR)} \qquad \text{(A1)}$$

Transverse electric (TE) mode has a vanished radial component, and the eigenmode is:

$$\frac{[n_1 kRj_l(n_1 kR)]'}{j_l(n_1 kR)} = \frac{[n_2 kRh_l(n_2 kR)]'}{h_l(n_2 kR)} \qquad \text{(A2)}$$

R is the radius of the sphere, n_1 is the refractive index of the sphere, n_2 is the refractive index of the environment outside the sphere. $k = 2\pi/\lambda$. k_l and h_l are the spherical bessel and hankel functions. The radiative quality factor Q_{rad} of a particular eigenmode is:

$$Q_{rad} = \frac{\mathrm{Re}[x]}{2\,\mathrm{Im}[x]} = \frac{n_1{}^2\sqrt{n_1{}^2 - n_2{}^2}\,\mathrm{Re}[x]}{2n_2{}^2 \exp[-2T]} \qquad \text{(A3)}$$

where x is the size parameter $x = 2\pi R/\lambda$. T is a variable that depends on x weakly; the radiative quality factor Q_{rad} therefore scales linearly with the size parameter:

$$Q_{rad} \propto x \qquad \text{(A4)}$$

To match the lasing modes observed experimentally with theoretical WGM values, we derived the asymptotic solutions for mode order p and mode number m following [17]:

$$\lambda^{-1}(R, n_1, n_r, p, m) = \frac{1}{2\pi R n_1}(m + \frac{1}{2} + 2^{-\frac{1}{3}}\alpha(p)(m+\frac{1}{2})^{\frac{1}{3}} - \frac{L}{(n_r{}^2 - 1)^{\frac{1}{2}}} + \frac{3}{10}2^{-\frac{2}{3}}\alpha^2(p)(m+\frac{1}{2})^{-\frac{1}{3}} - 2^{-\frac{1}{3}}L(n_r{}^2 - \frac{2}{3}L^2)\frac{\alpha(p)(m+\frac{1}{2})^{-\frac{2}{3}}}{(n_r{}^2-1)^{\frac{3}{2}}}) \quad \text{(A5)}$$

where $n_r = n_1/n_2$, $L = n_r^{-1}$ for TM modes, and $L = n_r$ for TE modes. $\alpha(p)$ are the roots of the Airy function.

Figure 1. a) shows a schematic diagram of the droplet laser. The width of the channel at the flow-focusing nozzle was 15 μm. The width of the channel was 60 μm at $y = 0$, and narrowed to 20 μm at $y = 16$ cm. The height of the channel (in the z-direction) was 43 μm. Drops containing 1 mM solution of rhodamine 640 perchlorate in benzyl alcohol dissolved into water as they travelled in the channel, and their sizes decreased. The concentration of rhodamine increased as the volume of the drops decreased. This effect on the emission spectrum from the droplet cavities was insignificant (see text). b) The droplets were optically excited by a pulsed frequency-doubled Nd:YAG at repetition rate of 1 kHz, much higher than the rate of generation of drops (~ 125 drops/second). The excitation beam was directed perpendicular to the plane of the microchannel (in the *z*-direction). The optical output from the drops was collected through an objective behind the channel in the same direction as the pump beam (*z*-direction). The dichroic mirror reflects light with wavelength at 532 nm, and transmits light with wavelengths > 532 nm.

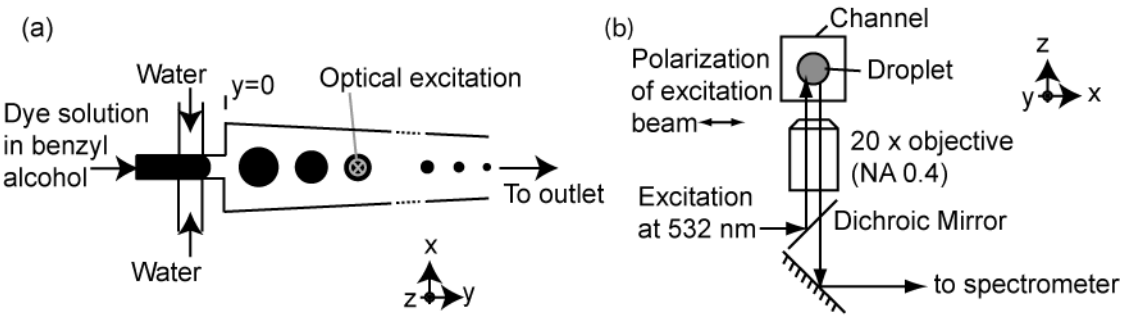

Figure 2. a) shows a snapshot of the device during its operation. b) shows the radius of the drops at different distances down the channel. The rate of flow of the carrier fluid was 200 μL h^{-1}, and that of the disperse phase was 20 μL h^{-1}. The insets show images of the drops at different positions in the channel. The image of the smallest drop appears smeared because the drop was moving faster than the frame rate of the camera. c) shows the surface area of the drops as a function of their residence time in the channel. The decrease in surface area follows a first-order kinetics with rate constant k = -0.92 s^{-1}. The R^2 value for the fit was 0.94.

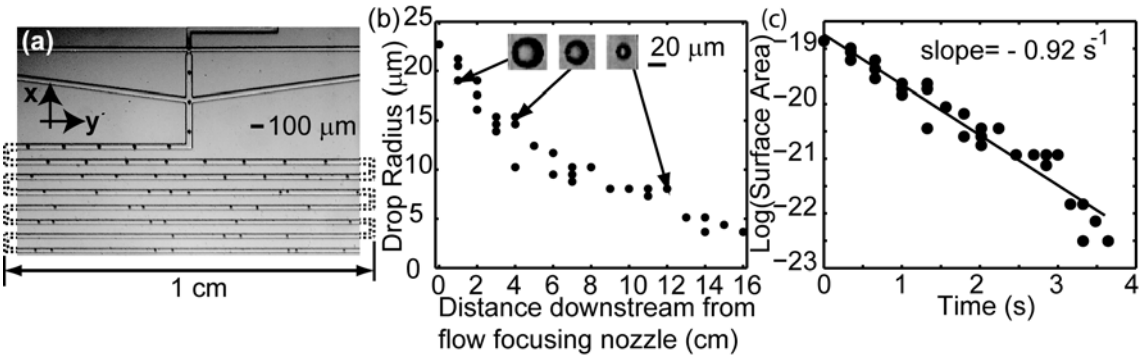

Figure 3. a) Optical micrographs of emitted light (> 600 nm) from a droplet with radius ~ 17.4 μm imaged in the *x*-*y* plane when illuminated (i) by a low-power (100 mW) continuous-wave green laser with energy below lasing threshold, and (ii) by a pulsed green laser (0.24 mJ/pulse) with energy above lasing threshold. The dotted line in (a)(i) shows the outline of the drop. (b) shows a rendering image of a spherical micro-cavity and the cross-section of a WGM field profile (p = 1, $m = l$ = 238), generated using finite element method (FEM) simulations. The radius of the cavity simulated was 17.352 μm. The index of the cavity was 1.54, and that in the surroundings was 1.33. (c) Absorption (solid line) and fluorescence spectra (dashed line) from rhodamine 640 perchlorate in benzyl alcohol. (d) Emission spectrum of a single droplet containing 1-mM solution of rhodamine 640 in benzyl alcohol at input pulse energy of 0.24 mJ/pulse, corresponding to the image in (a)(ii). The dashed line shows the fluorescence spectrum below lasing threshold, corresponding to the image in (a)(i). The calculated WGM positions for a spherical cavity with radius =17.352 μm for transverse magnetic modes with p = 1 to 3 and m = 230 to 250 were aligned above the lasing spectrum. The linewidth of the modes was 0.16 nm, close to the resolution limit of the spectrometer (0.1 nm). The inset shows the output intensity from the droplet integrated over wavelengths from 650 nm to 690 nm as a function of input pulse energy. The lasing threshold was about 2 μJ/pulse. The points in this inset were averages of 14 sets of data. The error bar equals to one standard deviation.

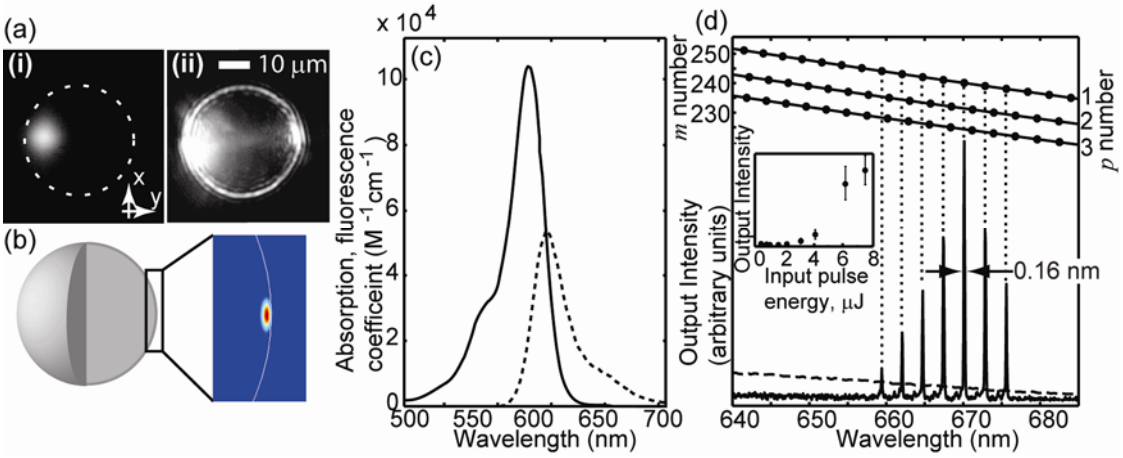
(a)
(i)
(ii)
10 μm
x
y
(b)
x 10^4
(c)
Absorption, fluorescence coefficeint (M^-1cm^-1)
Wavelength (nm)
(d)
m number
p number
Output Intensity (arbitrary units)
Input pulse energy, μJ
0.16 nm
Wavelength (nm)

Figure 4. a) Lasing spectra from drops possessing different radius *R*. The baseline value of each spectrum indicates the radius of the drop. The resolution of the spectrometer was 0.3 nm. b) Free spectral range (FSR) as a function of drop radius. The line was a fit to the data (Radius $R = c/(2\pi n_{eff} \times \mathrm{FSR})$, $n_{eff} = 1.48$). The R^2 value of the fit was 0.98.

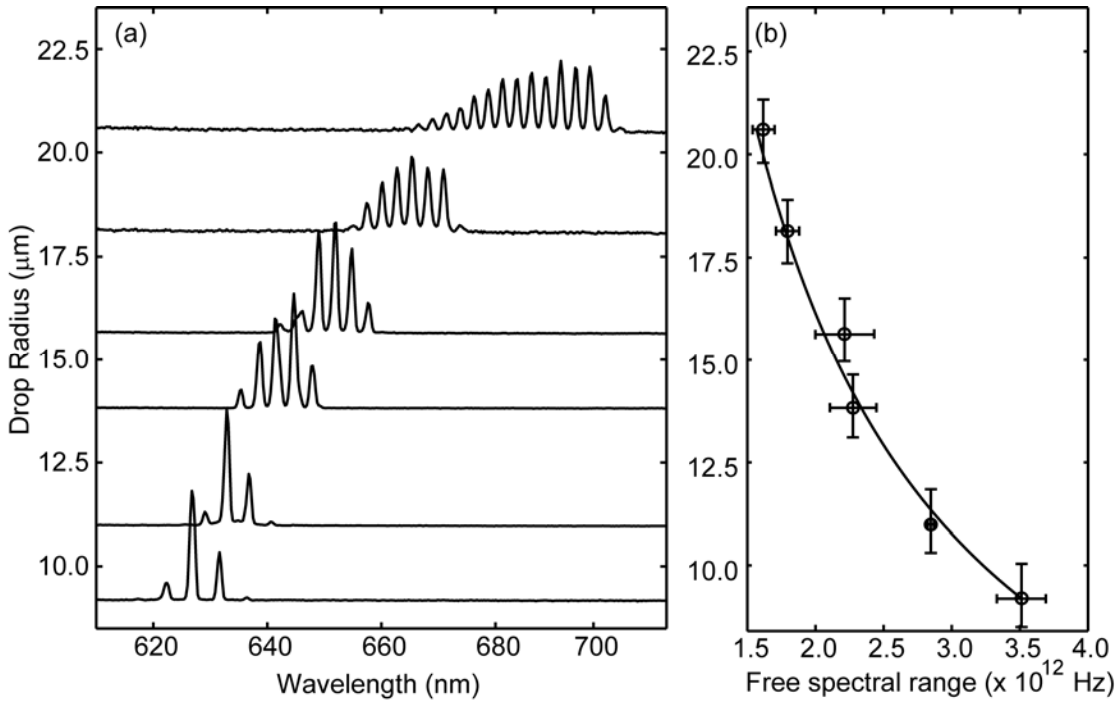

Figure 5. (a) Schematic diagram showing the gain spectrum (red) and the out-coupling efficiency β (black) of light from the droplet cavity. β shifts to shorter wavelengths as the radius of the cavity R decreases. (b) Schematic diagram showing the gain spectrum (red) and V/λ^3 (black), where V is the optical mode volume of the cavity. V/λ^3 shifts to shorter wavelengths as R decreases. (c) shows a diagram of the output power from the droplet laser. Since the output power is proportional to the product of the gain spectrum, the mode volume, and the out-coupling efficiency, the emission peak shifts to shorter wavelengths as the radius of the cavity decreases. (d) shows the calculated output power for droplet cavities with R = 8.9 μm and R = 19.4 μm respectively. The shift in the peak output power from λ_{peak} ~ 700 nm (for drops with R = 19.4 μm) to λ_{peak} ~ 600 nm (for drops with R = 8.9 μm) was approximately equal to that observed in Figure 4a.